Commun Nonlinear Sci Numer Simulat 14 (2009) 2982–2998

Contents lists available at ScienceDirect

Commun Nonlinear Sci Numer Simulat

journal homepage: www.elsevier.com/locate/cnsns

Effects of partial slip, viscous dissipation and Joule heating on Von Kármán flow and heat transfer of an electrically conducting non-Newtonian fluid

Bikash Sahoo *

Department of Mathematics, National Institute of Technology, Rourkela, Rourkela 769008, India

ARTICLE INFO

Article history:
Received 19 June 2008
Received in revised form 23 October 2008
Accepted 23 October 2008
Available online 11 November 2008

PACS:
47.15
47.50
47.65

Keywords:
Reiner–Rivlin fluid
MHD flow
Rotating disk
Partial slip
Heat transfer
Viscous dissipation
Joule heating
Finite difference method
Broyden's method

ABSTRACT

The steady Von Kármán flow and heat transfer of an electrically conducting non-Newtonian fluid is extended to the case where the disk surface admits partial slip. The fluid is subjected to an external uniform magnetic field perpendicular to the plane of the disk. The constitutive equation of the non-Newtonian fluid is modeled by that for a Reiner–Rivlin fluid. The momentum equations give rise to highly non-linear boundary value problem. Numerical solutions for the governing non-linear equations are obtained over the entire range of the physical parameters. The effects of slip, magnetic parameter and non-Newtonian fluid characteristics on the velocity and temperature fields are discussed in detail and shown graphically. Emphasis has been laid to study the effects of viscous dissipation and Joule heating on the thermal boundary layer. It is interesting to find that the non-Newtonian cross-viscous parameter has an opposite effect to that of the slip and the magnetic parameter on the velocity and the temperature fields.

© 2008 Elsevier B.V. All rights reserved.

1. Introduction

The flow of a viscous fluid which arises due to the rotation of a disk in an otherwise stagnant fluid constitutes a prototype of the three-dimensional boundary layer problems. It is seldom that one is able to find a closed form solution to the Navier–Stokes equations. The steady laminar flow of a viscous, incompressible fluid near a rotating disk is one of the few problems in fluid dynamics for which the Navier–Stokes equations admit an exact solution. The problem of disk flows has occupied a central position in the field of fluid dynamics. Disk flows have immediate technical applications in rotating machinery, heat and mass exchangers, biomechanics and oceanography. A disk of infinite extent is in the plane $z = 0$ and rotates with an angular velocity Ω about the z-axis (see Fig. 1) in an otherwise stagnant fluid. A boundary layer on each side of the disk develops, through which the tangential component of the velocity is sheared from the value Ωr at the surface to the value zero in the free stream outside the boundary layer. In practice, only the flow on one side of the disk ($z > 0$) needs to be discussed. The centrifugal forces created by the rotating disk cause a radial outflow of the fluid within the boundary layer. Since, the radial

* Tel.: +91 0661 246 2706.
E-mail address: bikashsahoo@nitrkl.ac.in

1007-5704/$ - see front matter © 2008 Elsevier B.V. All rights reserved.
doi:10.1016/j.cnsns.2008.10.021

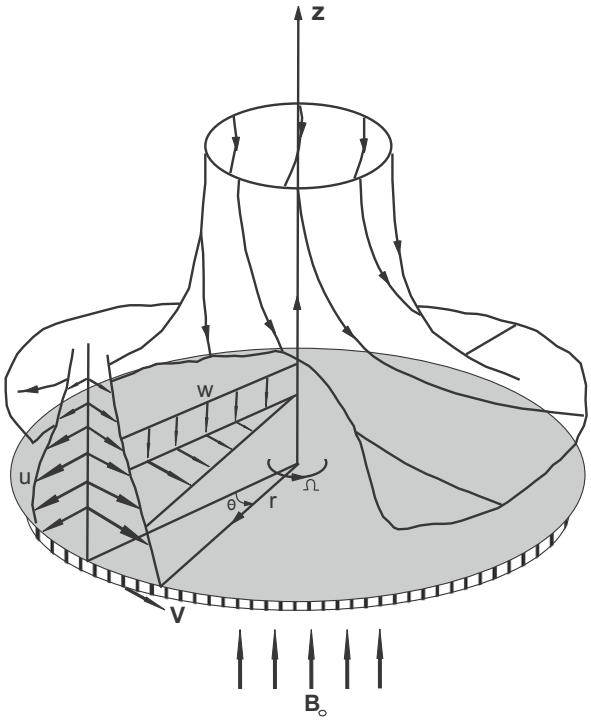

Fig. 1. Schematic representation of the flow domain.

component of the velocity is zero both on the disk ('no-slip' condition) and in the free stream, external fluid is entrained axially in to the boundary layer and ejected centrifugally again. This is therefore a fully three-dimensional flow which acts as a pump. The radial flow is often referred to as the '*free-disk pumping effect*'.

The theoretical study of the flow near a rotating disk can be traced back to the Von Kármán's similarity analysis [1]. That is why the flow is widely known as the Von Kármán flow. He devised an elegant similarity transformation which transforms the axisymmetric Navier–Stokes equations into a set of ordinary differential equations. There are few minor inaccuracies in Kármán's analysis, which were corrected by Cochran [2]. Stuart [3] studied the effects of uniform suction on the flow due to a rotating disk. Benton [4] improved the steady state solutions given by Cochran [2] and extended the problem to the transient state. The most accurate solution so far seems to have been reported by Ackroyed [5]. Due to its fundamental nature in combination with its practical importance, a vast number of modifications and extensions of Von Kármán's swirling flow problem exists. The classical problem has been generalized in several manners to include diverse physical effects. The heat transfer aspects have been considered by Millsaps and Pohlhausen [6] for variety of Prandtl numbers in the steady state. Sparrow and Gregg [7] studied the steady state heat transfer from a rotating disk maintained at a constant temperature to fluids at any Prandtl number. The rotationally symmetric flow of a viscous fluid in the presence of an infinite rotating disk has been considered by Rogers and Lance [8]. Later, Evans [9] has extended the study with uniform suction at the surface of the disk. The effects of uniform blowing on the flow induced by the rotating disk was studied by Kuiken [10]. The comprehensive review and detailed discussions by Owen and Rogers [11] gives an excellent overview of the flow phenomena occurring due to a single and two-disks systems. Attia [12] has adopted the Crank–Nicolson implicit method to find the solution of the system of non-linear differential equations arising due to the unsteady flow and heat transfer of a viscous incompressible fluid.

Technical applications of rotating disk problems can be found for instance in viscometry, spin-coating, manufacturing and use of computer disks, and in various rotating machinery components. In view of its wide applications in industrial and other technological fields, the problem of flow near a rotating disk has been extended to hydromagnetics. One of the major applications of the MHD rotating disk flow is the manufacture of the magnetic hard disk drives (HDD) with high information storage capacity [13]. The hydromagnetic flow due to a rotating disk was first investigated by Katukani [14]. Sparrow and Cess [15] have studied the MHD flow due to a rotating disk by incorporating the energy equation. In view of its immense applications, the flow problem continues to be studied till recently. Another reason for such an extensive study of the MHD flow due to a rotating disk may be due to the inherent problems in numerical integration of MHD equations, which typically lead to a general solution that includes two solutions, one exponentially growing and the other exponentially decaying. It would not be surprising that if the shooting techniques are employed, the actual numerical solution might be swamped by the parasitic solutions, no matter whether the integration is carried forward or backward. For this reason, apparently special measures need to be taken in numerical integration of the differential equations governing the flows in MHD, specially when the

strength of the magnetic field is not small and the flow is in infinite domain. Some interesting effects of the magnetic field on the steady and unsteady flows due to the rotation of a disk of infinite or finite extent have been examined by various authors [16–18].

In all of the above studies the fluid is assumed to be Newtonian. In recent years it has generally been recognized that in industrial applications non-Newtonian fluids are more appropriate than Newtonian fluids. That non-Newtonian fluids are finding increasing applications in industries has given impetus to many researchers. The Von Kármán flow of different kinds of non-Newtonian fluids have been studied by Srivastava [19], Jain [20], Mithal [21], Rathna [22], Elliott [23] and Ji et al. [24] including diverse physical effects. A detailed discussion up to 1991 regarding the flow of non-Newtonian fluids due to rotating disks can be found in the review paper by Rajagopal [25]. Ariel [26–28] has considered the flow of viscoelastic Walters 'B' and second grade fluids near a rotating disk. The Von Kármán flow of a non-Newtonian power-law fluid without and with a transverse magnetic field can be found in [29,30]. Recently, Attia [31–33] has considered the steady and unsteady Von Kármán flow and heat transfer of Reiner–Rivlin fluid with suction or injection at the surface of the disk.

Moreover, it is evident that [11] the flow arising due to the rotation of the single disk closely resembles the flow near the rotor in the rotor–stator system which has again vast industrial applications. Sahoo and Sharma [34] have studied the flow of a non-Newtonian second grade fluid in a rotor–stator system. The issue of paucity of boundary conditions has been addressed, and a numerical method has been adopted, which treats the higher order terms in the equations as lower iterates, essentially once again lowering the order of the equations.

In all the above mentioned studies, no attention has been given to the effect of partial slip on the flow due to a rotating disk. A completely different extension of Von Kármán's one disk problem is the analysis of Sparrow et al. [35]. They considered the flow of a Newtonian fluid due to the rotation of a porous surfaced disk and for that purpose replaced the conventional no-slip boundary conditions at the disk surface with a set of linear slip flow conditions. A substantial reduction in torque then occurred as a result of surface slip. A detailed account regarding the slip flow over an enclosed rotating disk can be found in the doctoral dissertation of Sarafa [36]. In fact, the surface of the disk may be rough and not perfectly smooth as assumed. In that case, the no-slip boundary condition becomes impractical to apply exactly. If the characteristic scale of the roughness is small compared to the boundary layer thickness on the disk, the no-slip condition may be approximated by partial slip condition applied to the envelop of the protuberances. The roughness may not be statistically isotropic. For example, it was found that for parallel, grooved surfaces the slip is larger in the direction along the grooves than the direction transverse to the grooves [37]. The work of Miklavčič and Wang [38] takes into consideration of the influence of partial slip on the flow of a viscous fluid due to a rotating disk. The effects of slip over a rotating disk in a Newtonian fluid lubricated by a non-Newtonian fluid has been considered by Andersson and Rousselet [39]. Further, one can refer the works of Attia [40], Asghar et al. [41], Frusteri and Osalusi [42] and Osalusi et al. [43] pertaining to the Von Kármán slip flow with diverse physical effects. Recently, Sahoo and Sharma [44] have investigated the effects of partial slip on the flow and heat transfer of a non-Newtonian Reiner–Rivlin fluid near a rotating disk. Their study reveals that the effects of slip is opposite to that of the non-Newtonian fluid parameter on the flow and heat transfer due to a rotating disk.

It seems that there has been relatively little information regarding the influence of partial slip on the flow of a non-Newtonian fluid due to a rotating disk. Further, few notable findings regarding the Kármán flow with slip boundary conditions which prompted for the present investigation are as follows.

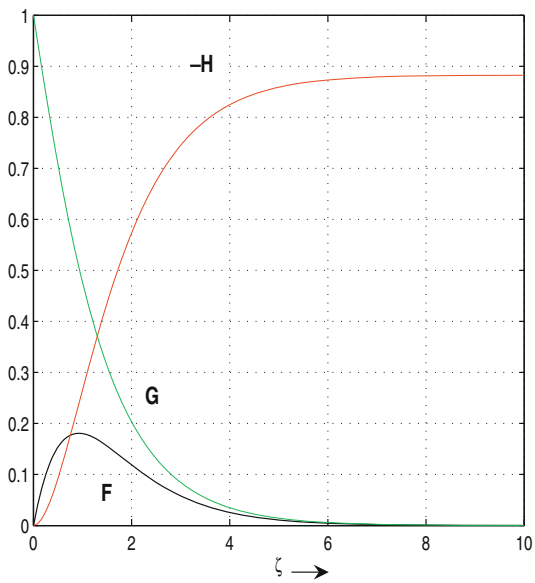

Fig. 2. Velocity profile for the Newtonian flow at $M_n = 0$ and $\lambda(= \eta) = 0$.

For the no-slip case (Kármán's original problem [1]) the radial velocity starts from zero and reaches a maximum near $\zeta = 0.92$, then decays to zero. But with partial slip Miklavčič and Wang [38] have reported that the maximum radial velocity decreases and its location moves towards the disk. They have also found that a cross over far away from the disk for the radial component of the velocity. The aforementioned findings are in agreement with those reported by Sahoo and Sharma [44] for non-Newtonian Reiner–Rivlin fluid in absence of magnetic field. Arikoglu and Ozkol [45] have observed that both the slip factor and the magnetic flux decrease the velocity in all directions and thicken the thermal boundary layer. Andersson and Rousselet [39] have found that the three-dimensional flow field is dramatically affected by accentuated velocity slip. They have reported that the axial flow towards the disk, i.e. the pumping efficiency and the torque required to maintain steady rotation of the disk, decrease monotonically with increasing slip. The MHD slip flow of a viscous Newtonian fluid over porous rotating disk, investigated by Frusteri and Osalusi [42] reveals that, the radial and the tangential velocity profiles are reduced by both slip coefficient and the magnetic field, whereas the axial velocity increases with an increase in the slip coefficient, contrary to the findings of [38,39,44].

Keeping the above curious findings in mind, the present work is devoted to examine the influence of partial slip, viscous dissipation and Joule heating on the steady Von Kármán flow and heat transfer of an electrically conducting non-Newtonian Reiner–Rivlin fluid. Emphasis has been given to the combined effects of the non-Newtonian fluid parameter, magnetic parameter and partial slip factor on the velocity and temperature fields. To the best of the author's knowledge, no attention has been given to the effects of slip on MHD boundary layer flow and heat transfer with viscous dissipation and Joule heating of a non-Newtonian Reiner–Rivlin fluid near a rotating disk. The obtained results have promising applications in engineering. This problem is not only important because of its technological significance but also in view of the interesting mathematical features presented by the equations governing the MHD slip flow and heat transfer.

2. Formulation of the problem

We consider an electrically conducting non-Newtonian Reiner–Rivlin fluid whose rheological behavior is governed by stress–strain rate law [46,47],

$$\tau^i_j = -p\delta^i_j + 2\mu e^i_j + 2\mu_c e^i_k e^k_j; \quad e^j_j = 0, \tag{1}$$

where p denotes the pressure, μ is the coefficient of viscosity, and μ_c is the coefficient of cross-viscosity. The fluid occupies the space $z > 0$ over an infinite rotating disk coinciding with the plane $z = 0$ (see Fig. 1). The disk is assumed to be rotating about z-axis with an uniform angular velocity Ω. The fluid adheres to the surface of the disk partially and thus, motion of the fluid exhibits the slip condition. An external uniform magnetic field is applied perpendicular to the plane of the disk and has a constant magnetic flux density B_0. The Lorentz force, included in the momentum equation can be simplified if the following assumptions are made:

- All physical quantities are constant.
- The induced magnetic field is small compared with the applied magnetic field.
- The electrical field is assumed to be zero.

These assumptions are valid when the magnetic Reynolds number is small and there is no displacement current Ref. [48]. It is natural to describe the flow in the cylindrical polar coordinates (r, ϕ, z). In view of the rotational symmetry, $\frac{\partial}{\partial\phi} \equiv 0$. The surface of the rotating disk is maintained at a uniform temperature T_w and far away from the wall, the free stream is kept at a constant temperature T_∞. Taking $\mathbf{V} = (u, v, w)$ for the steady flow,the equations of continuity and motion are,

$$\frac{\partial u}{\partial r} + \frac{u}{r} + \frac{\partial w}{\partial z} = 0, \tag{2}$$

and

$$\rho\left(u\frac{\partial u}{\partial r} + w\frac{\partial u}{\partial z} - \frac{v^2}{r}\right) + \sigma B_0^2 u = \frac{\partial \tau^r_r}{\partial r} + \frac{\partial \tau^z_r}{\partial z} + \frac{\tau^r_r - \tau^\phi_\phi}{r}, \tag{3}$$

$$\rho\left(u\frac{\partial v}{\partial r} + w\frac{\partial v}{\partial z} + \frac{uv}{r}\right) + \sigma B_0^2 v = \frac{\partial \tau^r_\phi}{\partial r} + \frac{\partial \tau^z_\phi}{\partial z} + \frac{2\tau^r_\phi}{r}, \tag{4}$$

$$\rho\left(u\frac{\partial w}{\partial r} + w\frac{\partial w}{\partial z}\right) = \frac{\partial \tau^r_z}{\partial r} + \frac{\partial \tau^z_z}{\partial z} + \frac{\tau^r_z}{r}. \tag{5}$$

The no-slip boundary conditions for the velocity field are given as

$$z = 0, \quad u = 0, \quad v = r\Omega, \quad w = 0, \tag{6a}$$

$$z \to \infty, \quad u \to 0, \quad v \to 0, \quad p \to p_\infty. \tag{6b}$$

By using the Von Kármán [1] transformations

$$u = r\Omega F(\zeta), \quad v = r\Omega G(\zeta), \quad w = \sqrt{\Omega\nu}H(\zeta), \quad z = \sqrt{\frac{\nu}{\Omega}}\zeta, \quad p - p_\infty = -\rho\nu\Omega P. \tag{7}$$

Eqs. (2)–(5) take the form

$$\frac{dH}{d\zeta} + 2F = 0, \tag{8}$$

$$\frac{d^2F}{d\zeta^2} - H\frac{dF}{d\zeta} - F^2 + G^2 - M_nF - \frac{1}{2}L\left[\left(\frac{dF}{d\zeta}\right)^2 - 3\left(\frac{dG}{d\zeta}\right)^2 - 2F\frac{d^2F}{d\zeta^2}\right] = 0, \tag{9}$$

$$\frac{d^2G}{d\zeta^2} - H\frac{dG}{d\zeta} - 2FG - M_nG + L\left(\frac{dF}{d\zeta}\frac{dG}{d\zeta} + F\frac{d^2G}{d\zeta^2}\right) = 0, \tag{10}$$

$$\frac{d^2H}{d\zeta^2} - H\frac{dH}{d\zeta} - \frac{7}{2}L\frac{dH}{d\zeta}\frac{d^2H}{d\zeta^2} + \frac{dP}{d\zeta} = 0, \tag{11}$$

where ζ is the non-dimensional distance measured along the axis of rotation, F, G, H and P are non-dimensional functions of ζ, ρ is the density, ν is the kinematic viscosity $\left(\nu = \frac{\mu}{\rho}\right)$ and σ is the electrical conductivity of the fluid. We define the magnetic interaction number M_n by $M_n = \frac{\sigma B_0^2}{\rho\Omega}$. The boundary conditions (6) become,

$$\zeta = 0: \quad F = 0, \quad G = 1, \quad H = 0, \tag{12a}$$

$$\zeta \to \infty: \quad F \to 0, \quad G \to 0, \quad P \to 0, \tag{12b}$$

where $L = \frac{\mu_c\Omega}{\mu}$ is the parameter that describes the non-Newtonian characteristic of the fluid. The above system (8)–(10) with the prescribed boundary conditions (12) are sufficient to solve for the three components of the flow velocity. Eq. (11) can be used to solve for the pressure distribution at any point if required.

A generalization of Navier's partial slip condition [38,49] gives, in the radial direction,

$$u|_{z=0} = \lambda_1\tau_r^z|_{z=0}, \tag{13}$$

and in the azimuthal direction

$$v|_{z=0} = \lambda_2\tau_\phi^z|_{z=0}, \tag{14}$$

where λ_1, λ_2 are, respectively the slip coefficients. Let

$$\lambda = \lambda_1\sqrt{\frac{\Omega}{\nu}}\mu \quad \eta = \lambda_2\sqrt{\frac{\Omega}{\nu}}\mu. \tag{15}$$

With the help of transformations (7) and Eq. (15), the partial slip boundary conditions (13) and (14) become

$$F(0) = \lambda[F'(0) - LF(0)F'(0)], \quad G(0) - 1 = \eta[G'(0) - 2LF(0)G'(0)], \quad H(0) = 0, \tag{16a}$$

$$F(\infty) \to 0, \quad G(\infty) \to 0. \tag{16b}$$

The governing equations are still Eqs. (8)–(10). The boundary conditions at infinity are Eq. (12b), but those on the disk are replaced by Eq. (16a). Theses boundary conditions imply that both radial (F), and tangential (G) components of velocity vanish sufficiently far away from the rotating disk, whereas the axial component of velocity (H) is anticipated to approach a yet unknown asymptotic limit for sufficiently large ζ value.

3. Heat transfer analysis

Due to the temperature difference between the surface of the disk and the ambient fluid, heat transfer takes place. The energy equation, with viscous dissipation and Joule heating takes the form,

$$\rho c_p\left(u\frac{\partial T}{\partial r} + w\frac{\partial T}{\partial z}\right) = \kappa\left\{\frac{1}{r}\frac{\partial}{\partial r}\left(r\frac{\partial T}{\partial r}\right) + \frac{\partial^2 T}{\partial z^2}\right\} + \mu\left[\left(\frac{\partial u}{\partial z}\right)^2 + \left(\frac{\partial v}{\partial z}\right)^2\right] + \sigma B_0^2(u^2 + v^2). \tag{17}$$

Introducing the non-dimensional variable $\theta(\zeta) = \frac{T - T_\infty}{T_w - T_\infty}$ and using the Von Kármán transformations (7), (17) becomes,

$$H\frac{d\theta}{d\zeta} = \frac{1}{P_r}\frac{d^2\theta}{d\zeta^2} + E_c(F'^2 + G'^2) + M_nE_c(F^2 + G^2), \tag{18}$$

where T_w is the temperature at the surface of the disk, T_∞ is the temperature of the ambient fluid at large distance from the disk, $P_r = \frac{\mu c_p}{\kappa}$ is the Prandtl number and $E_c = \frac{r^2\Omega^2}{(T_w - T_\infty)c_p}$ is the Eckert number. The boundary conditions in terms of the non-dimensional parameter θ are expressed as

$$\zeta = 0: \quad \theta = 1,$$
$$\zeta \to \infty: \quad \theta \to 0. \tag{19}$$

The heat transfer from the disk surface to the fluid is computed by the application of the Fourier's law, $q = -\kappa\left(\frac{\partial T}{\partial z}\right)_w$. Introducing the transformed variables, the expression for q becomes

$$q = -\kappa(T_w - T_\infty)\sqrt{\frac{\Omega}{\nu}}\frac{d\theta(0)}{d\zeta}. \tag{20}$$

By rephrasing the heat transfer results in terms of the Nusselt number defined as $N_u = \frac{q\sqrt{\frac{\nu}{\Omega}}}{\kappa(T_w - T_\infty)}$, we get

$$N_u = -\frac{d\theta(0)}{d\zeta}. \tag{21}$$

The action of the viscosity in the fluid adjacent to the disk tends to set up tangential shear stress $\bar{\tau}_\varphi$, which opposes the rotation of the disk. There is also a surface shear stress $\bar{\tau}_r$ in the radial direction. In terms of the variables of the analysis, the expressions of $\bar{\tau}_\varphi$ and $\bar{\tau}_r$ are respectively given as

$$\frac{\bar{\tau}_\phi}{\rho r\sqrt{\nu\Omega^3}} = \tau_\phi = \frac{dG(0)}{d\zeta} - 2LF(0)\frac{dG(0)}{d\zeta},$$
$$\frac{\bar{\tau}_r}{\rho r\sqrt{\nu\Omega^3}} = \tau_r = \frac{dF(0)}{d\zeta} - LF(0)\frac{dF(0)}{d\zeta}. \tag{22}$$

Although the above calculation is strictly speaking applicable to an infinite disk only, we may utilize the same results for a finite disk, provided the radius r is large enough. We shall now evaluate the most significant physical quantity of interest, the turning moment (or torque) for the disk with fluid on both sides. The dimensionless form of the moment coefficient is given by

$$C_m = \frac{-2\pi[G'(0) - 2LF(0)G'(0)]}{\sqrt{Re}}, \tag{23}$$

where $Re = \frac{r^2\Omega}{\nu}$ is the local rotational Reynolds number based on the radius and the tip velocity.

4. Numerical solution of the problem

The system of non-linear differential Eqs. (8)–(10) and (18) is solved under the boundary conditions (16) and (19), respectively. One can see that the initial boundary conditions for F and G in Eq. (16a) are unknown contrary to the case of no-slip boundary conditions (12a). Hence, the solution of the system can not proceed numerically using any standard integration routine. Here, we have adopted a second order numerical technique, similar to that of used in [44,50], which combines the features of the finite difference method and the shooting method. The method is accurate because it uses central differences. The semi-infinite integration domain $\zeta \in [0, \infty)$ is replaced by a finite domain $\zeta \in [0, \zeta_\infty)$. In practice, ζ_∞ should be chosen sufficiently large so that the numerical solution closely approximates the terminal boundary conditions (16b). If ζ_∞ is not large enough, the numerical solution will not only depend on the physical parameters L, M_n, λ, but also on ζ_∞. Hence, a finite value, large enough, has been substituted for ζ_∞, the numerical infinity, to ensure that the solutions are not affected by imposing the asymptotic conditions at a finite distance. The value of ζ_∞ has been kept invariant during the run of the program. The value of $\zeta_\infty = 10.0$ is found to be adequate to simulate $\zeta = \infty$ for all the cases shown in Figs. 3–22. However, for higher values of the flow parameters, the numerical integrations are performed over substantially larger domain to ensure that the outer boundary conditions at ζ_∞ are satisfied.

Now suppose we introduce a mesh defined by

$$\zeta_i = ih (i = 0, 1, \ldots, n), \tag{24}$$

h being the mesh size, and discretize Eqs. (8)–(10) and (18) using the central difference approximations for the derivatives, then the following equations are obtained.

$$\frac{F_{i+1} - 2F_i + F_{i-1}}{h^2} - H_i\left(\frac{F_{i+1} - F_{i-1}}{2h}\right) - F_i^2 + G_i^2 - M_nF_i$$
$$-\frac{1}{2}L\left[\left(\frac{F_{i+1} - F_{i-1}}{2h}\right)^2 - 3\left(\frac{G_{i+1} - G_{i-1}}{2h}\right)^2 - 2F_i\left(\frac{F_{i+1} - 2F_i + F_{i-1}}{h^2}\right)\right] = 0, \tag{25}$$

$$\frac{G_{i+1} - 2G_i + G_{i-1}}{h^2} - H_i\left(\frac{G_{i+1} - G_{i-1}}{2h}\right) - 2F_iG_i - M_nG_i$$
$$+L\left[\left(\frac{F_{i+1} - F_{i-1}}{2h}\right)\left(\frac{G_{i+1} - G_{i-1}}{2h}\right) + F_i\left(\frac{G_{i+1} - 2G_i + G_{i-1}}{h^2}\right)\right] = 0, \tag{26}$$

$$H_i\left(\frac{\theta_{i+1}-\theta_{i-1}}{2h}\right)-\frac{1}{P_r}\left(\frac{\theta_{i+1}-2\theta_i+\theta_{i-1}}{h^2}\right) - E_c\left[\left(\frac{F_{i+1}-F_{i-1}}{2h}\right)^2+\left(\frac{G_{i+1}-G_{i-1}}{2h}\right)^2\right]-M_nE_c(F_i^2+G_i^2)=0, \tag{27}$$

$$H_{i+1}=H_i-\frac{h}{2}(F_i+F_{i+1}). \tag{28}$$

Note that Eqs. (9), (10) and (18), which are written at ith mesh point, the first and second derivatives are approximated by the central differences centered at ith mesh point, while in Eq. (8), which is written at $(i+\frac{1}{2})$th mesh point, the first derivative is approximated by the difference quotient at ith and $(i+1)$th mesh points, and the right hand sides are approximated by the respective averages at the same two mesh points. This scheme ensures that the accuracy of $O(h^2)$ is preserved in the discretization.

Eqs. (25)–(27) are three term recurrence relations in F, G and θ, respectively. Hence, in order to start the recursion, besides the values of F_0, G_0 and θ_0, the values of F_1, G_1 and θ_1 are also required. These values can be obtained by Taylor series expansion near $\zeta=0$ for F, G and θ.

If

$$F'(0)=s_1,\quad G'(0)=s_2\quad\text{and}\quad\theta'(0)=s_3, \tag{29}$$

we have

$$\begin{aligned}F_1&=F(0)+hF'(0)+\frac{h^2}{2}F''(0)+O(h^2)\\G_1&=G(0)+hG'(0)+\frac{h^2}{2}G''(0)+O(h^2)\\\theta_1&=\theta(0)+h\theta'(0)+\frac{h^2}{2}\theta''(0)+O(h^2)\end{aligned} \tag{30}$$

The values $F(0)$, $G(0)$ and $\theta(0)$ are given as boundary conditions in (16) and (19). The values $F''(0)$, $G''(0)$ and $\theta''(0)$ can be obtained directly from (9), (10) and (18) and using the values in (29). After obtaining the values of F_1, G_1 and θ_1, the integration can now be performed as follows. H_1 can be obtained from (28). Using the values of H_1 in (25)–(27), the values of F_2, G_2 and θ_2 are obtained. At the next cycle, H_2 is computed from (28) and is used in Eqs. (25)–(27) to obtain F_3, G_3 and θ_3, respectively. The order indicated above is followed for the subsequent cycles. The integration is carried out until the values of F, G, H and θ are obtained at all the mesh points.

Note that we need to satisfy the three asymptotic boundary conditions (16) and (19). In fact, s_1, s_2 and s_3 are found by shooting method along with fourth order Runge–Kutta method so as to fulfil the free boundary conditions at $\zeta=\zeta_\infty$ in (16) and (19). The guesses on $F'(0)$, $G'(0)$ and $\theta'(0)$ can be improved by a suitable zero-finding algorithm. Here, amongst several choices, one can apply a variation of secant method or use Newton's method as the zero-finding algorithm. In Newton's method, one has to solve sixteen equations at each integration step (four original Eqs. (25)–(28) plus four equations resulting from taking partial derivatives with respect to each unknown s_1, s_2 and s_3). Again, the three-dimensional version of the secant method is quite sensitive to the initial guesses and require a lot more iterations. However, we found Broyden's [51,52] method quite adequate. The fact that the algorithm has an accuracy of only $O(h^2)$ need not concern us unduly, as we can easily hike the accuracy to $O(h^4)$ by invoking Richardson's extrapolation. With reasonably close trial values to start the iterations, the convergence to the actual values within an accuracy of $O(10^{-6})$ could be attained in 9–12 iterations.

Note that even though we have used finite difference scheme to approximate the derivatives, we are still using the shooting method to solve the present boundary value problem. In fact, the shooting method is straight forward and it works well for small values of the flow parameters, whereas a special merit of the algorithm reported in the present work is that it is applicable for arbitrary values of the flow parameters L, M_n and λ (or η).

It is customary to mention that the above solution procedure belongs to one of the major classes of solution strategies for BVPs Refs. [53,54].

5. Results and discussion

The method described above was translated into a FORTRAN 90 program and was run on a pentium IV personal computer. The value of ζ_∞, the numerical infinity has been taken large enough and kept invariant through out the run of the program. To see if the program runs correctly, the results of $F'(0)$, $-G'(0)$ and $F_{\max}$ for the viscous fluid ($L=0$) subject to no-slip boundary conditions ($\lambda=\eta=0$), are compared (see Table 1) with the exact solutions reported by Ariel [17], for different values of the magnetic parameter. The comparison is found to be in good agreement. In order to have an insight of the flow and heat transfer characteristics, results are plotted graphically in figures for the uniform roughness ($\lambda=\eta$), different choice of the non-dimensional magnetic and non-Newtonian parameters. Moreover, the values of the important standard parameters like $-H_\infty$, τ_r, τ_ϕ, C_m and N_u have been tabulated in Table 2, for different values of the flow parameters when $P_r=1.0$, $E_c=0.3$ and $Re=4.0$.

Fig. 2 represents the corresponding velocity profile for the no-slip Newtonian ($L = 0$) flow at $M_n = 0$. It is clear that in absence of slip, the radial velocity F starts from zero and reaches a maximum near $\zeta = 0.92$ and then decays to zero.

Table 1
Variations of $F'(0)$, $-G'(0)$ and F_{max} with M_n for $L = 0$ and $\lambda(= \eta) = 0$.

M_n	$F'(0)$		$-G'(0)$		F_{max}	
	Current result	Ariel [17]	Current result	Ariel [17]	Current result	Ariel [17]
0.0	0.510214	0.510233	0.615909	0.615922	0.180740	0.180767
0.2	0.453137	0.453141	0.708794	0.708795	0.146343	0.146361
0.4	0.405575	0.405576	0.802376	0.802376	0.119166	0.119254
0.6	0.366698	0.366698	0.894475	0.894476	0.098445	0.098537
0.8	0.335090	0.335090	0.983607	0.983607	0.082841	0.082842
1.0	0.309259	0.309258	1.069053	1.069053	0.070756	0.070873
10.0	0.105310	0.105310	3.164907	3.164907	0.008312	0.008316
12.0	0.096163	–	3.466103	–	0.006923	–
14.0	0.089045	–	3.743246	–	0.005924	–
16.0	0.083303	–	4.001301	–	0.005203	–
18.0	0.078545	–	4.243731	–	0.004623	–
20.0	0.074518	0.074518	4.473067	4.473067	0.004164	–
50.0	0.047139	0.047139	7.071303	7.071303	0.001650	–
100	0.033334	0.033333	10.000083	10.000083	0.000833	–

Table 2
Variations of $-H_\infty$, τ_r, τ_ϕ, C_m, and N_u with different flow parameters.

L	M_n	$\lambda(= \eta)$	$-H_\infty$	τ_r	τ_ϕ	C_m	N_u
0.0			0.137633	0.037059	−0.513095	1.611937	0.093298
5.0			1.053198	0.152564	−0.205124	0.644416	0.332981
10.0	1.0	1.0	1.453484	0.091378	−0.098222	0.308573	0.304438
15.0			1.731162	0.063418	−0.065318	0.205204	0.283069
20.0			1.963864	0.048376	−0.049116	0.154302	0.266871
	0.0		1.158215	0.188433	−0.313511	0.984923	0.478983
	5.0		0.123879	0.075839	−0.642264	2.017733	0.074471
2.0	10.0	1.0	0.053750	0.049252	−0.731521	2.298140	0.056219
	15.0		0.031972	0.036892	−0.775719	2.436993	0.055849
	20.0		0.021903	0.029676	−0.803170	2.523233	0.057714
		0.0	1.266822	0.923505	−0.914327	2.872442	0.365162
		10.0	0.000906	0.000094	−0.096926	0.304502	0.099538
2.0	1.0	20.0	0.000083	0.000006	−0.049447	0.155342	0.099877
		30.0	0.000020	0.000001	−0.033132	0.104088	0.099950
		40.0	0.000007	0.000000	−0.024902	0.078231	0.099974

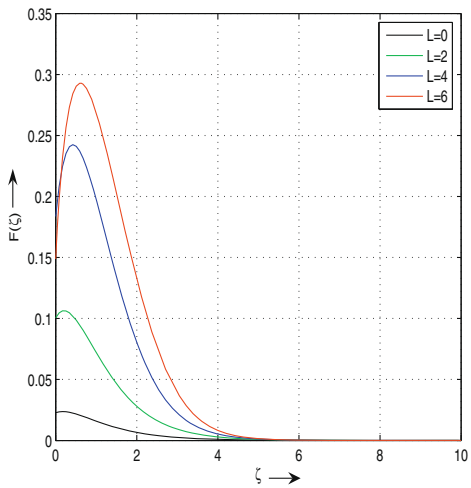

Fig. 3. Variation of F with L at $M_n = 1.0$ and $\lambda(= \eta) = 2.0$.

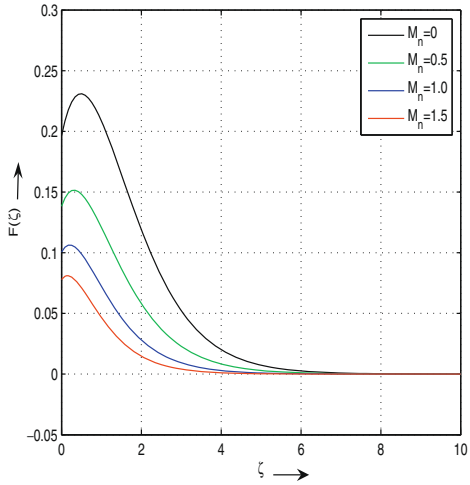

Fig. 4. Variation of F with M_n at $L = 2.0$ and $\lambda(= \eta) = 2.0$.

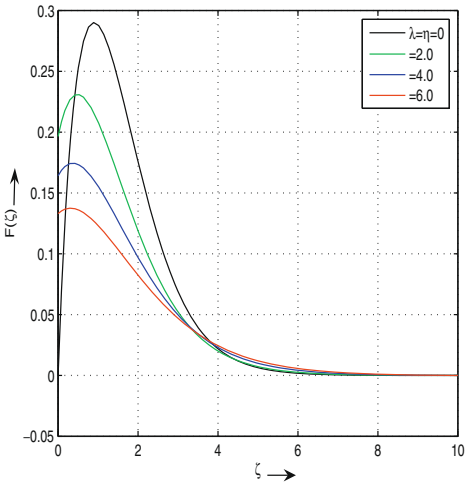

Fig. 5. Variation of F with $\lambda(= \eta)$ at $L = 2.0$ and $M_n = 0$.

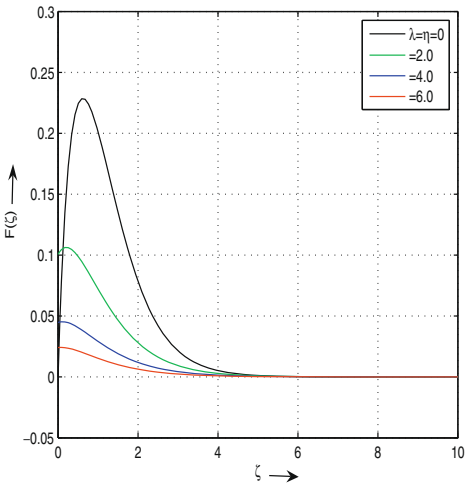

Fig. 6. Variation of F with $\lambda(= \eta)$ at $L = 2.0$ and $M_n = 2.0$.

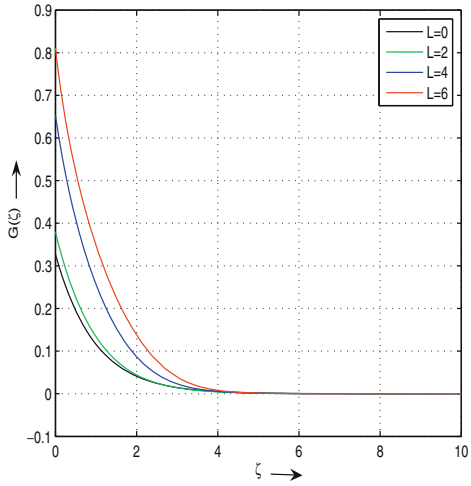

Fig. 7. Variation of G with L at $M_n = 1.0$ and $\lambda(= \eta) = 2.0$.

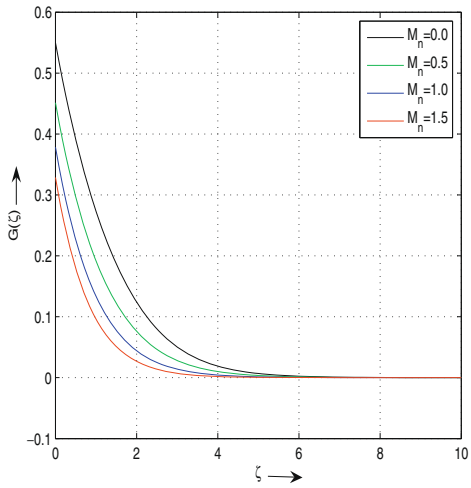

Fig. 8. Variation of G with M_n at $L = 2.0$ and $\lambda(= \eta) = 2.0$.

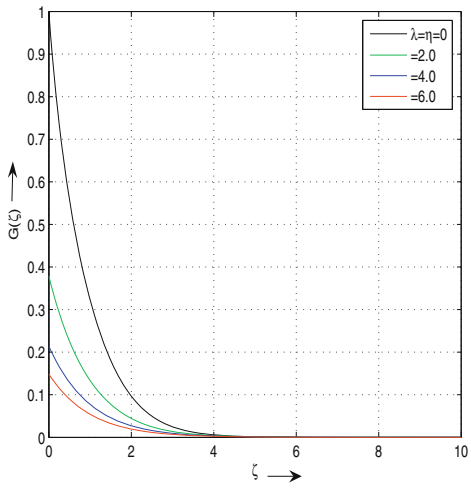

Fig. 9. Variation of G with $\lambda(= \eta)$ at $L = 2.0$ and $M_n = 2.0$.

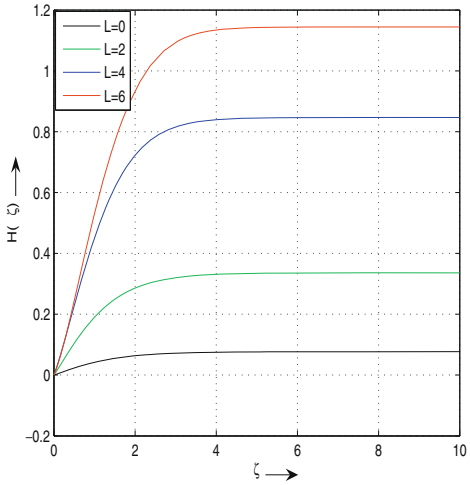

Fig. 10. Variation of $-H$ with L at $M_n = 1.0$ and $\lambda(=\eta) = 2.0$.

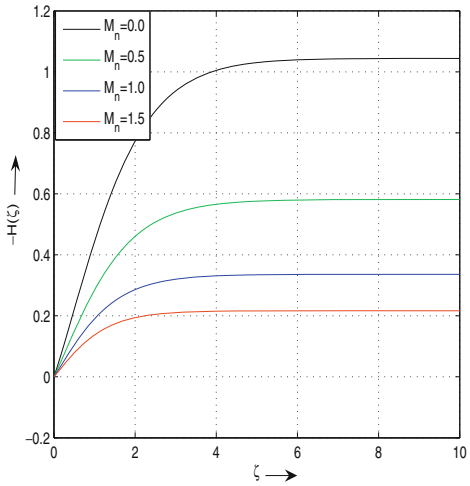

Fig. 11. Variation of $-H$ with M_n at $L = 2.0$ and $\lambda(=\eta) = 2.0$.

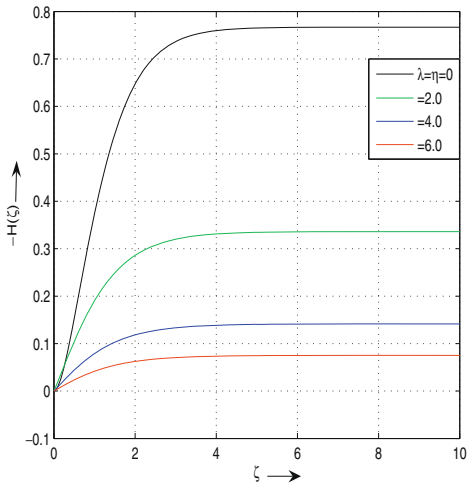

Fig. 12. Variation of $-H$ with $\lambda(=\eta)$ at $L = 2.0$, $M_n = 2.0$.

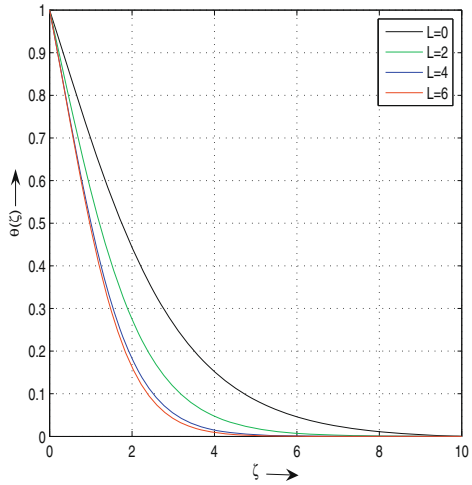

Fig. 13. Variation of θ with L at $M_n = 0.1$, $\lambda(=\eta) = 2.0$, $Pr = 1.0$ and $E_c = 0.3$.

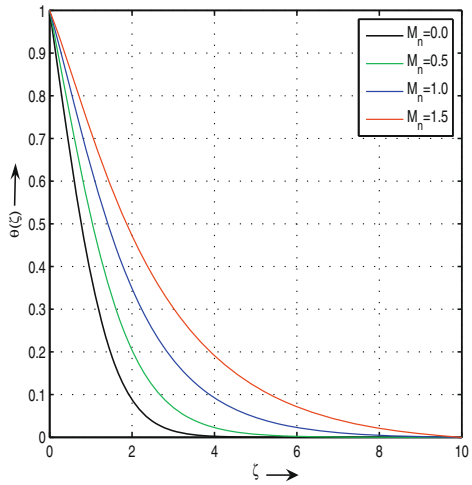

Fig. 14. Variation of θ with M_n at $L = 2.0$, $\lambda(=\eta) = 2.0$, $Pr = 1.0$ and $E_c = 0.3$.

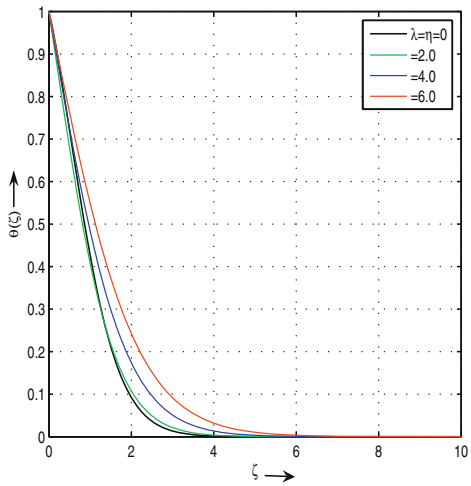

Fig. 15. Variation of θ with $\lambda(=\eta)$ at $L = 2.0$, $M_n = 0.1$, $P_r = 2.0$ and $E_c = 0.3$.

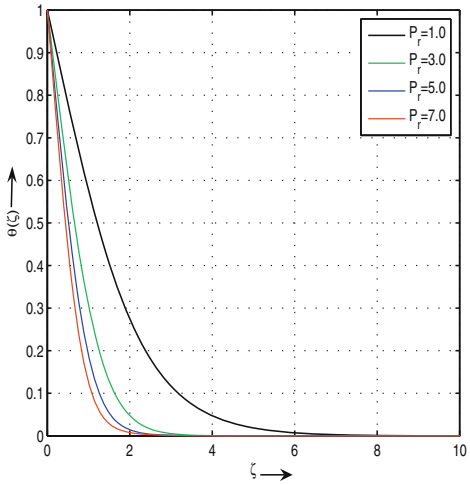

Fig. 16. Variation of θ with P_r at $L = 2.0$, $M_n = 0.1$, $\lambda(= \eta) = 2.0$ and $E_c = 0.3$.

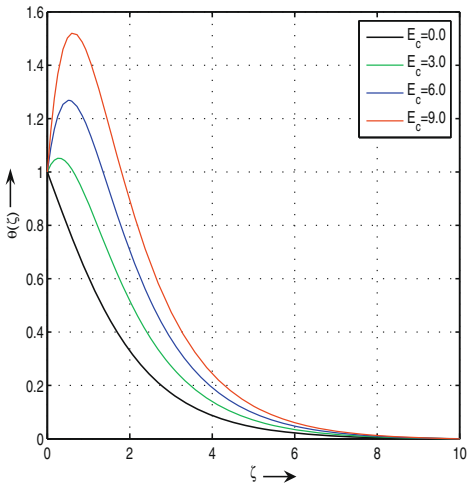

Fig. 17. Variation of θ with E_c at $L = 2.0$, $M_n = 1.0$, $\lambda(= \eta) = 2.0$ and $P_r = 2.0$.

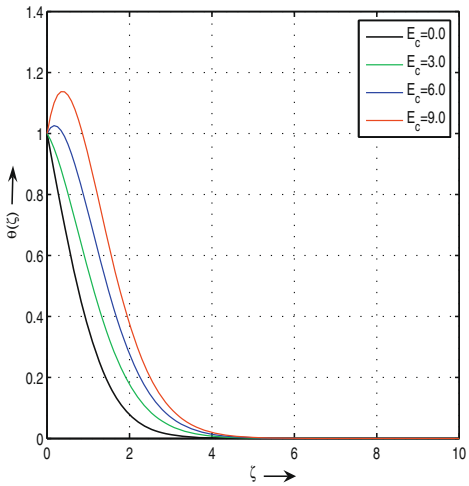

Fig. 18. Variation of θ with E_c at $L = 2.0$, $M_n = 0$, $\lambda(= \eta) = 2.0$ and $P_r = 2.0$.

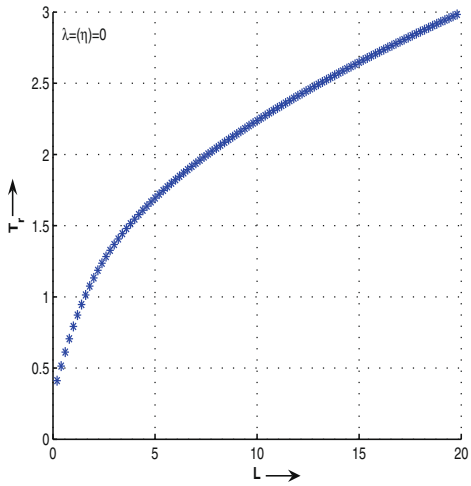

Fig. 19. Variation of τ_r with L at $M = 1.0$ and $\lambda(= \eta) = 0$.

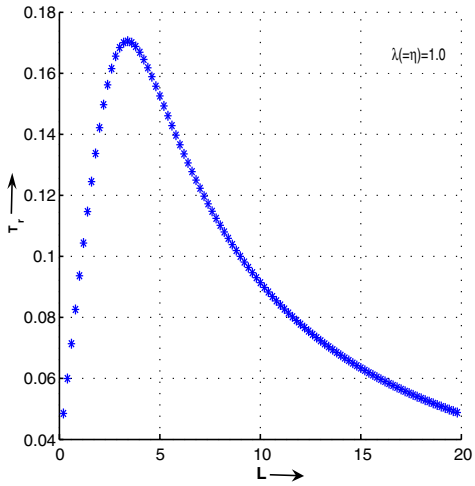

Fig. 20. Variation of τ_r with L at $M = 1.0$ and $\lambda(= \eta) = 1.0$.

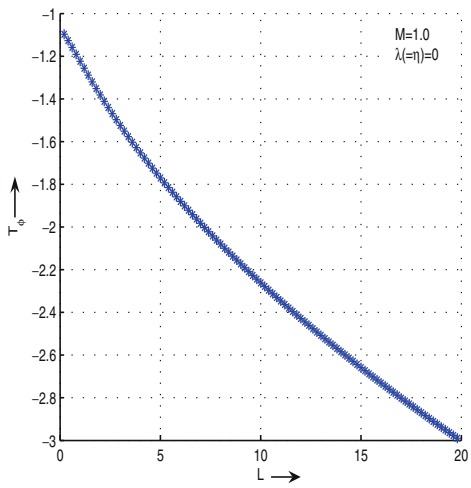

Fig. 21. Variation of τ_ϕ with L at $M = 1.0$ and $\lambda(= \eta) = 0$.

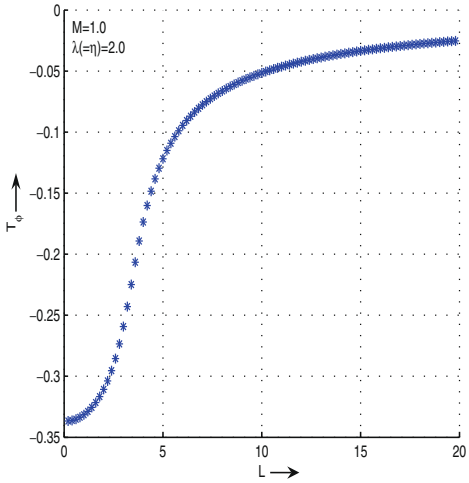

Fig. 22. Variation of τ_ϕ with L at $M = 1.0$ and $\lambda(= \eta) = 2.0$.

Figs. 3–6 respectively depict the variations of the radial component of velocity $F(\zeta)$ as a function of ζ for different values of the non-Newtonian parameter L, magnetic parameter M_n, and the slip factor $\lambda(= \eta)$. It is observed that (see Fig. 3) for a given position ζ, in presence of slip, $F(\zeta)$ increases with L, and hence, the maximum value of the radial component $F_{\max}$ increases. From Fig. 4, it is clear that $F(\zeta)$ decreases with an increase in the magnetic parameter M_n due to the inhibiting influence of the Lorentz force. Figs. 5 and 6 delineate that slip has a prominent effect on the radial component of the velocity near the disk. As the slip parameter increases in magnitude, permitting more fluid to slip past the disk, the maximum radial velocity decreases and its location moves towards the disk. Fig. 5 depicts, in absence of the magnetic field, a prominent cross over of the curves $F(\zeta)$ is observed near $\zeta = 4.0$, showing although slip decreases the radial component of velocity near the disk, it increase the velocity far from the disk. This cross over was also observed by Miklavčič and Wang [38] for a viscous fluid; Sahoo and Sharma [44] for the non-Newtonian Reiner–Rivlin fluid without magnetic field. However, it is interesting to find that as the magnetic parameter M_n increases, the position of the cross over shifts towards the ζ axis and finally coincides with it, as is clear from Fig. 6. In the limiting case as $\lambda(= \eta) \to \infty$, i.e. when the fluid is entirely potential, the rotating disk has no effect to rotate the fluid particles, and therefore, the fluid becomes at rest.

In Figs. 7 and 8 we plot the dimensionless azimuthal component of velocity $G(\zeta)$ as a function of ζ with L and M_n, respectively. The figures show that the shear driven motion $G(\zeta)$ in the azimuthal direction decays rapidly with the distance ζ from the disk. Its value in general increases with an increase in the value of L, but decreases as the magnetic field is increased. That is Lorentz force, which opposes the flow leads to enhanced deceleration of the azimuthal velocity. Fig. 9 depicts that the slip has a prominent effect on G near the disk and for a given position ζ, $G(\zeta)$ decreases with an increase in the slip factor $\lambda(= \eta)$.

Figs. 10–12 show the axial velocity profiles $-H(\zeta)$ with different flow parameters. From the figures, it is clear that the axial component of velocity increases with an increase in the non-Newtonian parameter L and decreases with the magnetic parameter M_n. As pointed out earlier, due to the rotation of the disk, the layer near the surface is thrown outwards owing to the action of the centrifugal force. This is compensated by particles which flow in an axial direction $(-H)$ towards the disk, to be in turn carried and ejected centrifugally. The gradual reduction of the peak in the F-profiles in Fig. 6 with increasing values of the slip parameter is reflected in the distributions of the axial velocity component in Fig. 12. The distinct inflection point in the $-H$-profiles for higher values of $\lambda(= \eta)$ seems to gradually disappear. This is a consequence of the direct coupling between the radial and the axial velocity components through the continuity constraint (8). The reduction of the radial velocity $F(\zeta)$ with increasing $\lambda(= \eta)$ automatically gives rise to a reduced axial inflow since,

$$-H(\infty) = 2\int_0^\infty F d\zeta. \tag{31}$$

The variation of the non-dimensional temperature profiles $\theta(\zeta)$ with different flow parameters are shown in Figs. 13–18. From Fig. 13 it is clear that for a given position ζ, the temperature decreases with an increase in the non-Newtonian parameter L. On the other hand, the magnetic and the slip parameters have opposite effects on the temperature profile. Since the magnitude of the increase of thermal boundary layer thickness due to the magnetic parameter M_n is more appreciable than that decreased due to the non-Newtonian parameter L, we can expect that the thermal characteristics are more influenced by M_n than those by L in this problem. In Fig. 15, one can observe that as the slip parameter increases, the temperature gets increased, resulting in a increase in the thermal boundary layer thickness. Fig. 16 shows the variation of the temperature with the Prandtl number P_r. As was expected, θ gets decreased with an increase in P_r, and thus, the thermal boundary layer thickness gets decreased. In fact, it is well known that the thermal boundary layer thickness is inversely proportional to the square root of Prandtl number. Hence, the decrease of temperature profile with P_r is straightforward.

The heat generated due to the Joule heating and viscous dissipation are characterized by M_n and E_c respectively. In Figs. 17 and 18, we plot $\theta(\zeta)$ with the Eckert number E_c, when the other flow parameters are kept constant. The inclusion of Joule heating $M_n \neq 0$ has a prominent effect on the temperature distribution, as is clear from Fig. 17. The effects of Joule heating on the thermal characteristics at the surface of the disk are magnified when E_c becomes large. In both of the aforementioned figures, one can observe that there is a temperature overshoot near the disk, with an increase in the Eckert number. This is of course a consequence of the fact that for higher values of the Eckert number, there is significant generation of heat due to viscous dissipation near the disk, so that the temperature in the region very close to the disk exceeds T_w.

Variations of the radial component of velocity at ζ_∞, (i.e. $-H_\infty$), the non-dimensional radial shear stress (τ_r), the tangential shear stress (τ_ϕ), and the Nusselt number with different values of the flow parameters have been tabulated in Table 2. The inflow rate at infinity, as one can see form this Table, decreases both with the slip factor and the magnetic interaction number. This is quite natural since the radially outwards boundary layer is fed by the axial flow at infinity. The effect of the magnetic field is to reduce and eventually suppress (Fig. 4) the radially directed out flow. An accompanying reduction of the axial flow (Fig. 11) towards the disk is observed together of the thinning of the boundary layer adjacent to the disk, there by increasing the torque (C_m) (see: Table 2) required to maintain rotation of the disk at the prescribed angular velocity. It is observed from Table 2 that an increase in the slip parameter substantially reduces the radial and the tangential shear stresses τ_r and τ_ϕ. One of the novel findings (see Table 2 and Fig. 20) of the present investigation is that in presence of the slip factor, the radial shear stress τ_r initially increases with the non-Newtonian parameter L, reaches its maximum value (critical value not precisely determined), and then starts falling. However, such a turning point is not observed for the no-slip case (Fig. 19). Similarly, Figs. 21 and 22 reveal interesting effects of the slip on the tangential shear stress τ_ϕ. Moreover, an increase in the magnetic interaction parameter M_n, surprisingly decreases the Nusselt number N_u, and hence, the heat transfer rate from the surface of the disk to the ambient fluid up to certain value of M_n, and then the Nusselt number starts increasing with M_n, as is clear from Table 2.

6. Conclusions

This work is a worthwhile attempt to study of the effects of partial slip, viscous dissipation and Joule heating on the flow and heat transfer of an electrically conducting non-Newtonian Reiner–Rivlin fluid due to a rotating disk. The new set of slip flow boundary conditions aimed to accommodate for the partial slip effect. An effective second order numerical scheme has been adopted to solve the resulting system of highly non-linear differential equations subject to the slip boundary conditions. The use of *Broyden's method* has indeed enhanced the efficiency of the present algorithm by reducing the computational (CPU) time. The combined effects of the slip and the magnetic interaction parameter are studied in detail. It is interesting to find that the non-Newtonian cross-viscous parameter L has an opposite effect to that of the slip and the magnetic parameter on the velocity and the temperature fields. The inclusion of viscous dissipation and Joule heating have prominent effects on the thermal boundary layer. Moreover, for the slip flow, a turning point in curve presenting the non-dimensional radial shear stress (τ_r) has been found, which is absent for the no-slip case.

Acknowledgements

The suggestions made by the anonymous reviewers to improve the quality of the work are highly acknowledged.

References

[1] Von Kármán Th. Über laminare und turbulente reibung. Z Angew Math Mech, ZAMM 1921;1:233–52.
[2] Cochran WG. The flow due to a rotating disk. Proc Camb Phil Soc 1934;30:365–75.
[3] Stuart JT. On the effects of uniform suction on the steady flow due to a rotating disk. Quart J Mech Appl Math 1954;7:446–57.
[4] Benton ER. On the flow due to a rotating disk. J Fluid Mech 1966;24:781–800.
[5] Ackroyd JAD. On the steady flow produced by a rotating disc with either surface suction or injection. J Eng Math 1978;12:207–20.
[6] Millsaps K, Polhausen K. Heat transfer by laminar flow from a rotating plate. J Aero Sci 1952;19:120–6.
[7] Sparrow EM, Gregg JL. Heat transfer from a rotating disk to fluids of any Prandtl number. J Heat Trans ASME 1959;81:249–51.
[8] Rogers MH, Lance GN. The rotationally symmetric flow of a viscous fluid in the presence of an infinite rotating disk. J Fluid Mech 1960;7:617–31.
[9] Evans DJ. The rotationally symmetric flow of a viscous fluid in the presence of an infinite rotating disk with uniform suction. Quart J Mech Appl Math 1969;XXII:467–85.
[10] Kuiken HK. The effect of normal blowing on the flow near a rotating disk of infinite extent. J Fluid Mech 1971;47:789–98.
[11] Owen JM, Rogers RH. Flow and heat transfer in rotating disk systems. Research Stud. Press Ltd, John Wiley & Sons; 1989.
[12] Attia HA. On the effectiveness of uniform suction–injection on the unsteady flow due to a rotating disk with heat transfer. Int Commun Heat Mass Transfer 2002;29:653–61.
[13] Cho HH, Won CH, Ryu GY, Rhee DH. Local heat transfer characteristics in a single rotating disk and co-rotating disks. Micro Syst Tech 2003;9:399–408.
[14] Katukani T. Hydromagnetic flow due to a rotating disk. J Phys Soc Jpn 1962;17:1496–506.
[15] Sparrow EM, Cess RD. Magnetohydrodynamic flow and heat transfer about a rotating disk. J Appl Mech Trans ASME 1962;29:181–7.
[16] Attia HA. Unsteady MHD flow near a rotating porous disk with uniform suction or injection. Fluid Dyn Res 1998;23:283–90.
[17] Ariel PD. On computation of MHD flow near a rotating disk. Z Angew Math Mech, ZAMM 2002;82:235–46.
[18] Attia HA, Aboul-Hassan AL. On hydromagnetic flow due to a rotating disk. Appl Math Model 2004;28:1007–14.
[19] Srivastava AC. Rotation of a plane lamina in non-Newtonian fluids. Bull Calc Math Soc 1958;50:57–67.
[20] Jain MK. The flow of a non-Newtonian liquid near a rotating disk. Appl Sci Res 1961;10:410–8.
[21] Mithal KG. On the effects of uniform high suction on the steady flow of a non-Newtonian liquid due to a rotating disk. Quart J Mech Appl Math 1961;XIV:403–10.

[22] Rathna SL. Flow of a particular class of non-Newtonian fluid near a rotating disk. Z Angew Math Mech, ZAMM 1962;42:232–7.
[23] Elliott L. Elastico-viscous flow near a rotating disk. Phys Fluid 1971;14:1086–90.
[24] Ji Z, Rajagopal KR, Szeri AZ. Multiplicity in solutions in Von Kármán flows of viscoelastic fluids. J Non-Newtonian Fluid Mech 1990;36:1–25.
[25] Rajagopal KR. Flow of viscoelastic fluids between rotating disks. Theor Comp Fluid Dyn 1992;3:185–206.
[26] Ariel PD. A hybrid method for computing the flow of viscoelastic fluids. Int J Numer Meth Fluid 1992;14:757–74.
[27] Ariel PD. On the flow of an elastico-viscous fluid near a rotating disk. J Comp Appl Math 2003;154:1–25.
[28] Ariel PD. Computation of flow of a second grade fluid near a rotating disk. Int J Eng Sci 1997;35:1335–57.
[29] Andersson HI, de Korte E, Meland R. Flow of a power-law fluid over a rotating disk revisited. Fluid Dyn Res 2001;28:75–88.
[30] Andersson HI, de Korte E. MHD flow of a power-law fluid over a rotating disk. Eur J Mech B: Fluid 2002;21:317–24.
[31] Attia HA. Steady Von Kármán flow and heat transfer of a non-Newtonian fluid with uniform suction or injection. Int Commun Heat Mass Transfer 2003;30:871–9.
[32] Attia HA. Numerical study of flow and heat transfer of a non-Newtonian fluid on a rotating porous disk. Appl Math Comp 2005;163:327–42.
[33] Attia HA. Numerical study of flow and heat transfer in a Reiner–Rivlin fluid on a rotating porous disk. J Appl Mech Tech Phys 2005;46:68–76.
[34] Sahoo B, Sharma HG. Numerical investigation of flow of a non-Newtonian fluid in a rotor–stator system. In: Proceedings of the 9th annual CFD symposium, CFD Div AeSI, Bangalore, India; 2006.
[35] Sparrow EM, Beavers GS, Hung LY. Flow about a porous surfaced rotating disk. Int J Heat Mass Transfer 1971;14:993–6.
[36] Sarafa ZN. Slip flow over an enclosed rotating disk. PhD thesis, University of Illinois, Urbana-Champaign; 1963.
[37] Wang CY. The Stokes drag due to the sliding of a smooth plate over a finned plate. Phys Fluid 1994;6:2248–52.
[38] Miklavčič M, Wang CY. The flow due to a rough rotating disk. Z Angew Math Phys, ZAMP 2004;55:235–46.
[39] Andersson HI, Rousselet M. Slip flow over a lubricated rotating disk. Int J Heat Fluid Flow 2006;27:329–35.
[40] Attia H. On the effectiveness of ion-slip on steady MHD flow and heat transfer above a rotating disk with Ohmic heating. J Fluid Eng 2006;128:1236–9.
[41] Asghar S, Hanif K, Hayat T. The effect of the slip condition on unsteady flow due to non-coaxial rotations of disk and a fluid at infinity. Meccanica 2007;42:141–8.
[42] Frusteri F, Osalusi E. On MHD and slip flow over a rotating porous disk with variable properties. Int Commun Heat Mass Transfer 2007;34:492–501.
[43] Osalusi E, Side J, Harris R, Johnston B. On the effectiveness of viscous dissipation and Joule heating on steady MHD flow and heat transfer of a Bingham fluid over a porous rotating disk in the presence of Hall and ion-slip currents. Int Commun Heat Mass Transfer 2007;34:1030–40.
[44] Sahoo B, Sharma HG. Effects of partial slip on steady Von Kármán flow and heat transfer of a non-Newtonian fluid. Bull Braz Math Soc 2007;38:595–609.
[45] Arikoglu A, Ozkol I. On the MHD and slip flow over a rotating disk with heat transfer. Int J Numer Meth Heat Fluid Flow 2006;16:172–84.
[46] Reiner M. A mathematical theory of dilatency. Am J Math 1945;67:350–62.
[47] Schowalter WR. Mechanics of non-Newtonian fluids. Pergamon press; 1978.
[48] Shercliff JA. A text book of magnetohydrodynamics. Oxford: Pergamon Press; 1965.
[49] Navier CLMH. Sur les lois du mouvement des fluides. Mem Acad R Acad R Sci Inst Fr 1827;6:389–440.
[50] Sahoo B. Hiemenz flow and heat transfer of a third grade fluid. Commun Non-linear Sci Numer Simulat 2008;14:811–26.
[51] Broyden CG. A class of methods for solving non-linear simultaneous equations. Math Comput 1965;19:577–93.
[52] Broyden CG. On the discovery of the "good Broyden method". Math Prog Ser B 2000;87:209–13.
[53] Keller HB. Numerical methods for two-point boundary value problems. New York: Dover Publishing Inc.; 1992.
[54] Ascher UM, Mattheij RMM, Russell RD. Numerical solution of boundary value problems for ordinary differential equations. Philadelphia: SIAM; 1995.